RESIDUAL STRAIN MEASUREMENT IN THERMAL BARRIER COATINGS

Thomas R. Watkins, Scott P. Beckman [†] and Camden R. Hubbard

Oak Ridge National Laboratory
P.O. Box 2008
Oak Ridge, TN 37831-6064

ABSTRACT

The residual strain states in the top coat and bond coat of a thermal barrier coating system were measured as a function of depth in as-received and heat treated (200 hrs at 1150 °C in air) conditions using an x-ray diffraction/layer removal technique. The specimens consisted of electron beam assisted physical vapor deposited, yttria -stabilized zirconia top coat on a René N5 superalloy substrate with a "PtAl" bond coat in-between the two. Both the as-received and heat treated specimens showed little in-plane strain except near the top coat/bond coat interface where the tetragonal ZrO_2 phase became more compressive. After heat treatment, the in-plane residual strains in the cubic ZrO_2 phase were observed to be tensile.

INTRODUCTION

Thermal barrier coatings (TBC's) have been developed to improve component life and performance in engines, particularly in gas turbine engines, by providing additional thermal protection for the metallic components. Generically, the coupled use of improved alloys and TBC's has increased the turbine operating temperatures by 120 °C over the past four decades [1], allowing current combustion gas temperatures to reach 1300 °C. Industrial interest in TBC technology is significant as the total value of coatings has been reported at $1.7 and $1.5 billion for vapor deposited and plasma-spray coatings, respectively [1].

A TBC system typically consists of a ceramic top coat, a metallic bond coat, and a metal substrate (see Figure 1). The top coat provides thermal insulation to the metallic portions of the part and is typically a yttria stabilized zirconia (YSZ) which possesses a low thermal conductivity, a high thermal expansion coefficient and a low Young's modulus. Generally, the top coat is deposited by either electron beam assisted physical vapor deposition (EB-PVD) or thermal spray methods resulting in a columnar or lamellar microstructures, respectively. The resultant top coat properties depend on both the material properties and the microstructure, especially defects [2,3]. The metallic bond coat provides oxidation and corrosion protection and is typically composed of (Pt,Ni)Al or MCrAlY (M = metal). Upon exposure to oxidizing high

[†] Currently at the Department of Materials Science and Engineering, Iowa State University, 3053 Gilman Hall, Ames, IA 50011

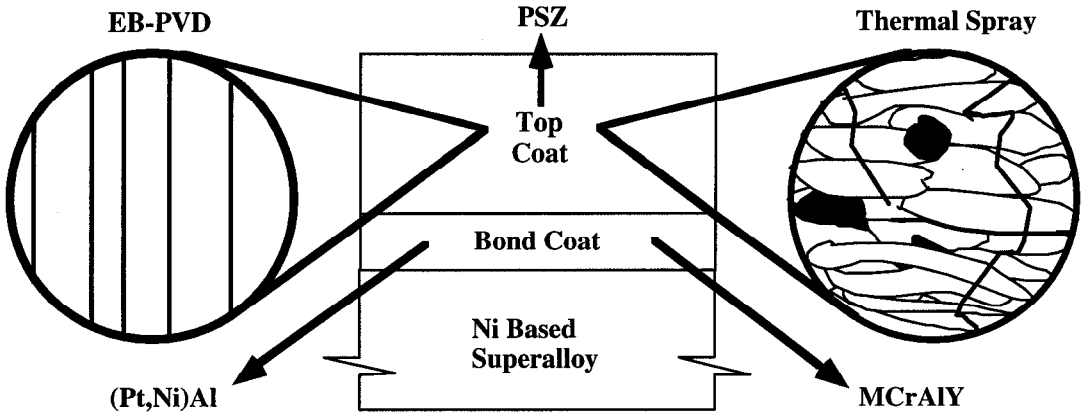

Figure 1. Schematic of a typical TBC system. The insets indicate the microstructure of the EB-PVD or thermal spray YSZ layers

temperature environments, the bond coat is oxidized, via oxygen transport through the ZrO_2 top coat, forming an adherent alumina scale. Ideally, this scale acts as a barrier to further diffusion enhanced oxidation and corrosion. The bond coat is typically deposited by either chemical vapor deposition with ensuing thermal treatment (e.g., (Pt,Ni)Al) or a spraying process resulting in a diffusion coating, also called an overlay coating (e.g., MCrAlY). Substrate materials can vary widely from steel to superalloys. In aircraft engines, advanced substrates are Ni based, single crystal superalloys.

In service, spallation of the top coat typically occurs near the top coat/bond coat interface due to continuous oxide scale growth. In TBC systems with EB-PVD top coats, spallation failure typically occurs at the top coat/bond coat interface. While in TBC systems with top coats deposited via plasma-spray, this failure typically occurs within the top coat, near the top coat/bond coat interface [4]. Thus, understanding the nature of the oxide scale, especially residual stresses or strains within them, is critical to enhancing the performance and reliability of TBC systems. The purpose of this study is to investigate the residual strain state in the top coats and bond coats of an EB-PVD YSZ top coat/(Pt,Ni)Al bond coat/René N5 single crystal substrate specimens before and after heat treatment.

EXPERIMENTAL PROCEDURE

Table I lists the details of the experimental conditions for the x-ray measurements. In order to maximize intensity, a 4-axis (Φ, χ, Ω, 2Θ) goniometer [5] was employed for the strain measurements using the "Ω-goniometer geometry" [6(A)] (see Figure 2). The (420), (620) and (640) reflections from the tetragonal YSZ, cubic YSZ and Al_2Pt phases, respectively, were utilized for strain measurement. During scanning, the specimens were oscillated ±2 mm in plane to improve particle statistics. In order to obtain strain information as a function of depth, a layer removal technique via polishing was employed.

Specimen alignment was accomplished using a dial gauge probe which was accurate to ±5 μm. Here, the relative distance to the center of rotation is known, and the diffracting surface is positioned accordingly. The average strain free interplanar spacing, d_0, was determined from the x-ray data employing the analysis of Hauk et al. [6(B)]. Goniometer alignment was ensured by examining LaB_6 powder on a zero background plate. The maximum observed peak shift for

Table I - Experimental conditions of the x-ray measurements.

Parameter	Condition
Equipment	Scintag PTS goniometer MAC Science 18 kW rotating anode generator Scintag thermoelectrically-cooled Si(Li) detector
Power	10.5 kW; 35 kV, 300 mA
Radiation	Cu $K\alpha_1$, λ = 1.54059 Å
Incidence slit divergence	0.35°
Receiving slit acceptance	0.25°; radial divergence limiting (RDL) Soller slit
Source to specimen distance	360 mm
Specimen to back slit distance	280 mm
Tilt axis and angles	Ω; 0, ±28.2, ±42, ±55 ° (equal steps of $\sin^2\psi$)
Azimuthal angles	0, 45, 90°
2Θ Scans	0.02 °2Θ/step; 10 s/step

the (510) reflection of LaB_6 (141.7 °2Θ) was less than 0.01 °2Θ for Ω tilting as described in Table I.

The strains were calculated using the Dölle-Hauk method [6(C)] initially assuming a triaxial strain state. In order to more accurately estimate the standard deviations of the measurements, the seven scans of the (420) tetragonal YSZ and (620) cubic YSZ reflections were made at ψ = +55°. After each scan, the sample was oscillated briefly to change position, then rescanned and finally profile fit with a pseudo Voigt function. The standard deviations of peak positions were 0.011° and 0.020°, respectively. These were taken to apply to all tilt and azimuthal angles as has been done previously [7] and propagated through the Dölle-Hauk method to give standard deviations of strain.

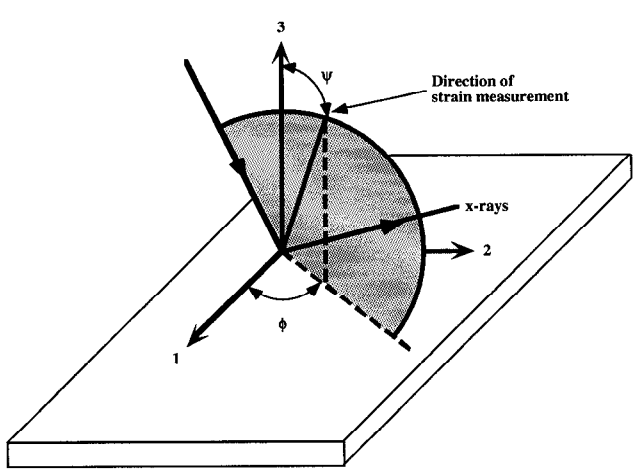

Figure 2. Schematic of diffraction conditions and definition of measurement axes with respect to the sample surface. Note that the incident and diffracted x-rays, the surface normal and direction of strain measurement were all coplanar in these experiments (i.e., Ω tilting).

SPECIMENS

Two EB-PVD YSZ top coat/(Pt,Ni)Al bond coat/René N5 specimens[††] were examined in as-received and heat treated (200 hrs at 1150 °C in air) conditions. In addition, one (Pt,Ni)Al bond coat/René N5 specimen in the as-received condition was also examined. The thicknesses of the top coat, bond coat, and substrate were 0.37-0.38, 0.05, and 1.6 mm, respectively. The nominal composition of the YSZ was 7-8 wt% Y_2O_3-ZrO_2. The nominal composition of the René N5 single crystal superalloy substrate was 63.07 Ni - 7.5 Co - 7.0 Cr - 6.5 Ta - 6.2 Al - 5.0 W - 3.0 Rh - 1.5 Mo - 0.16 Hf- 0.05 C - 0.02 Ti (wt%). Table II lists the phases found in the top surfaces of the aforementioned specimens using x-ray diffraction prior to polishing. The lattice parameter values found here were in agreement with those found by Hammond and Cocking [8]. The top coats exhibited limited texture. During layer removal, no monoclinic ZrO_2 was observed except for a trace amount in one of eight θ-2θ scans. The relative amounts of cubic and tetragonal phase for each specimen were roughly estimated using the ratio of the intensities of the cubic (620) and tetragonal (420) reflections, as peak overlap precluded using other analyses [9]. The as-received and heat treated specimens had about 9 and 10 % cubic phase, respectively.

Table II - Phases present in top surfaces of the top coats and bond coats.

Location	Phase	Lattice Parameters (Å)		PDF Card # [10]
		a	c	
Top Coat	Tetragonal YSZ	3.62	5.17	38-1437
	Cubic YSZ	5.13		30-1468
Bond Coat	Al_2Pt	5.90		3-1006
	AlNi	2.90		44-1188

STRAIN-FREE INTERPLANAR SPACING

The strain-free interplanar spacing, d_0, is of critical importance to any triaxial strain calculation as the magnitude of the strains will change dramatically with small changes in this parameter (< 0.01%). The strain-free interplanar spacings for the two specimens examined were calculated from the diffraction data using the analysis of reference 6(B) and are displayed in Figure 3 as a function of depth. Here, d_0 is relatively constant in the as-received sample until a depth of 350 μm, where it increases rapidly near the top coat/bond coat interface for both the tetragonal and cubic phases. After heat treatment, this variation with depth effectively vanished, producing d_0 values very close to those observed in the as-received specimen at depths >350μm. This suggests that a near interface chemistry variation was removed by yttria diffusion. Measured d_0 values of 0.8086 and 0.8163 Å were obtained from a crushed as-received top coat for the (420) tetragonal and (620) cubic reflections, respectively. However, uniform use of these values at all depths resulted in erroneously large ε_{33} values near the interface.

[††] G.E. Aircraft Engines, Cincinnati, OH.

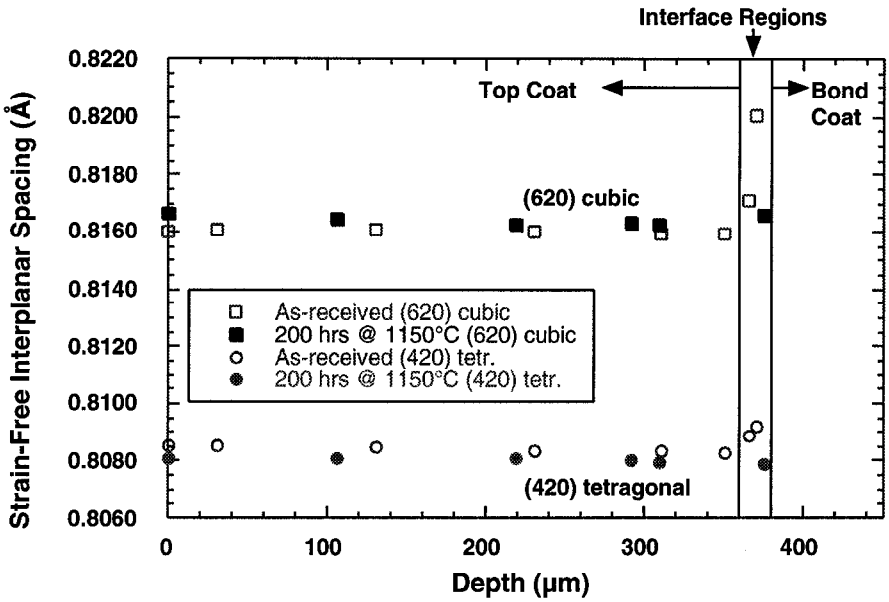

Figure 3. Strain-free interplanar spacing as a function of depth. The interface regions of the two specimens were combined here to give total thickness of 20 μm.

MICROSTRUCTURE

Representative microstructures of the as-received and heat treated specimens show that the top coats possess a columnar microstructure with numerous voids/cracks along most of the

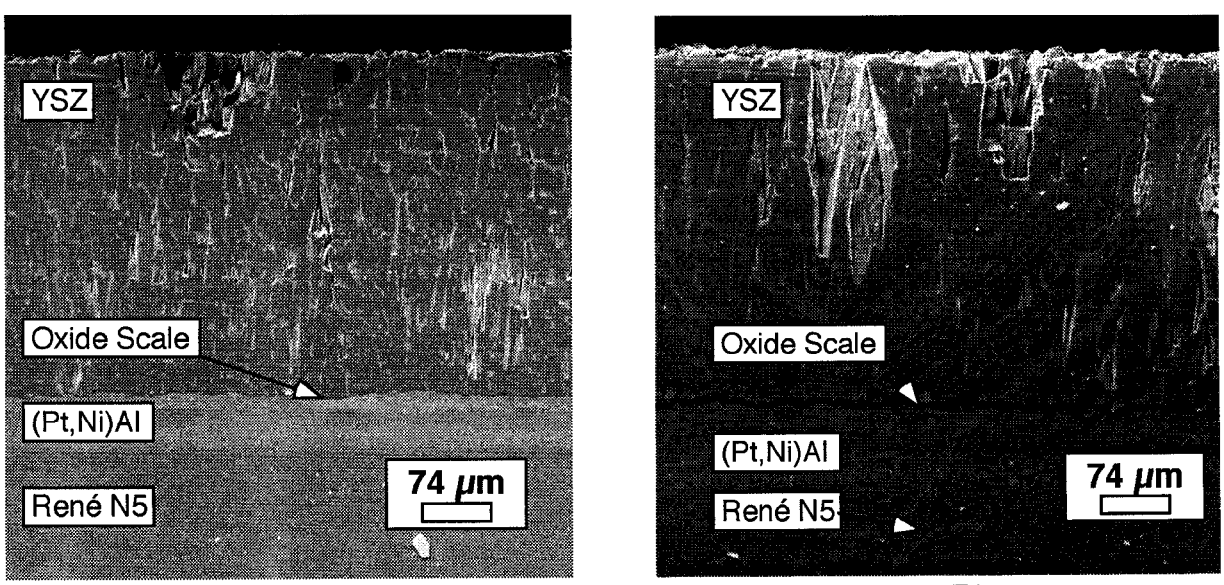

(A) (B)

Figure 4. Secondary electron micrographs of polished cross-sections of the as-received (A) and heat treated specimens (B) showing the YSZ top coat, oxide scale, (Pt,Ni)Al bond coat and René N5 superalloy base substrate.

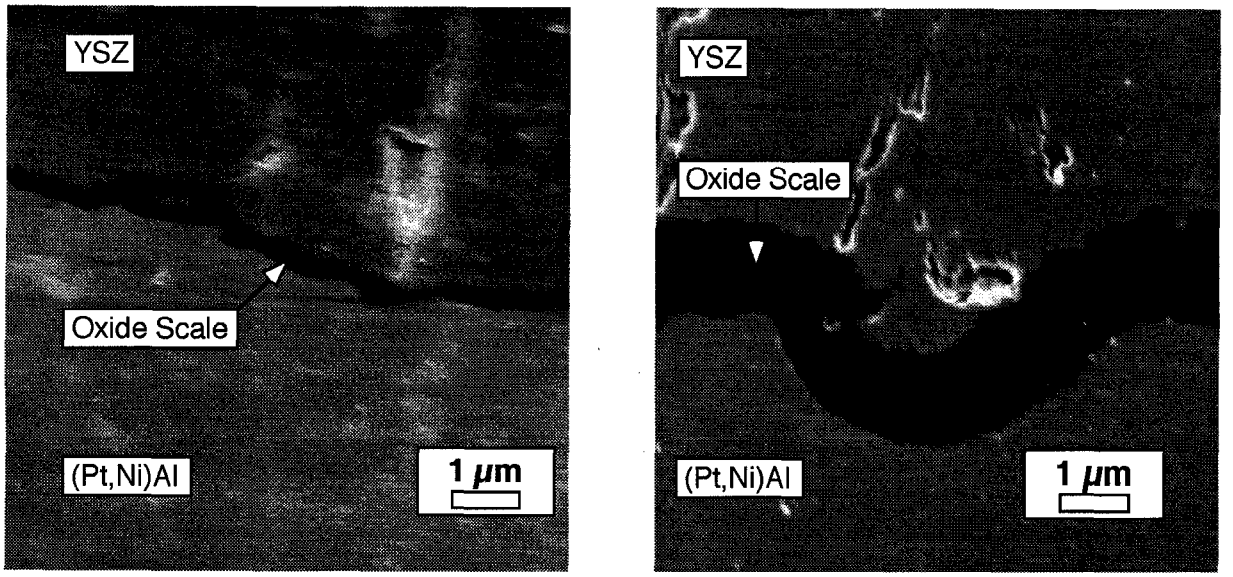

(A) (B)

Figure 5. Secondary electron micrographs of polished cross-sections of the as-received (A) and heat treated specimens (B) showing a close-up view of the top coat/oxide scale/bond coat interface.

columns (see Figure 4). The columns, cracks and grain boundary porosity are generally perpendicular to the top coat/bond coat interface, suggesting a very compliant top coat in-plane. The grain structure of the top coat appears coarser after heat treatment indicating that some sintering has occurred and providing a possible explanation for the change in d_0 near the interface. Further, the stratification of the bond coat near the top coat/bond coat interface has also clearly changed with heat treatment. In Figure 5, the thickness of the oxide scale at the top coat/bond coat interface is 1 μm in the as-received specimen and 4 μm in the heat treated

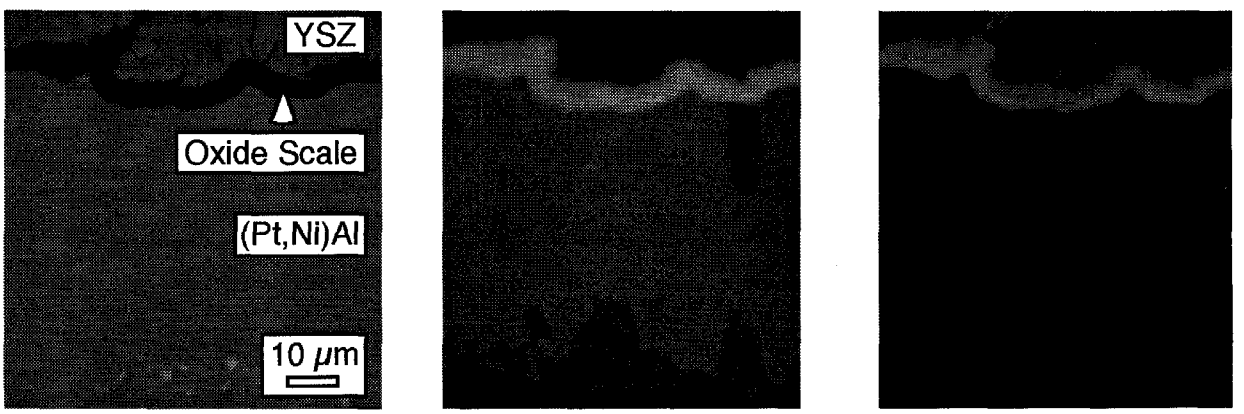

(A) (B) (C)

Figure 6. Micrographs from an atomic microprobe showing the regions of aluminum (B) and oxygen (C) concentrations relative to the backscattered electron image (A) of a polished cross-section of the heat treated specimen. In (B) and (C), regions of light/white contrast indicate high concentrations of the element relative to micrograph.

specimen. Figure 6 shows the results of wavelength and energy dispersive spectroscopy indicating that the dark feature resembling a crack in Figures 4 and 5 is actually a layer of predominantly Al_2O_3, which was also observed in the heat treated sample at a depth of 375 μm via x-ray diffraction. This alumina layer is also present in the as-received sample due to preoxidation, which occurred prior to ZrO_2 deposition.

RESIDUAL STRAINS

Figures 7 and 8 show the total residual strain (macro + micro) in each phase as a function of depth for the as-received and heat treated specimens, respectively. The lines defining the interface region in Figures 7 and 8 indicate that diffraction peaks from both the top coat and bond coat were observed at these depths. This is probably due to inherent roughness of the interface as well as the fact that the polishing was not perfectly parallel to the interface. For clarity, only the error bars for the ε_{11} and ε_{12} components are shown, representative of the other normal and shear strain components, respectively.

The plotted strains are uncorrected for the effects of layer removal. A simplified analysis was performed [11] to estimate the effect of layer removal upon the strains. Intuitively, as the coating is polished away, the constraint upon the metallic substrate is reduced allowing it to contract, which applies more compressive force on the remaining coating. As expected, the correction increased with depth making the strain in the tetragonal phase less compressive. Near the interface the measured strains were estimated to be roughly twice the actual strains. A more rigorous correction needs to be developed.

In Figures 7A, 7B, 8A and 8B, the measured residual strain states for the as-received and heat treated tetragonal YSZ are very similar. Here, the in-plane strains (ε_{11}, ε_{12}, ε_{22}) in the tetragonal YSZ were very small but quickly became compressive near the top coat/bond coat interface. Similarly, ε_{33} was very small but quickly became tensile near the top coat/bond coat interface. The magnitudes of ε_{11}, ε_{22}, and ε_{33} were nearly equal throughout the thickness of the top coat suggesting the superposition of macro and micro residual strain states. The out-of-plane shear strains (ε_{13}, ε_{23}) were very small throughout the thickness of the top coat. The ε_{11} and ε_{22} were nearly equal, suggesting that the porous/columnar nature of in-plane microstructure dominates. The only difference between the stain states is that the strains start to increase at a shallower depth (~220 μm) in the heat treated specimen than the as-received (~300 μm).

In Figures 7C and 8C, the measured residual strain states for the as-received and heat treated cubic YSZ are very different. For the as-received specimen, the strain state of the cubic YSZ exhibits in-plane tension which quickly becomes highly compressive near the top coat/bond coat interface. Similarly, ε_{33} exhibits out of plane compression which quickly becomes tensile near the top coat/bond coat interface. However, after heat treatment, the cubic ZrO_2 is in a tensile plane strain condition. Although this is possible as the cubic phase is the minority phase and probably discontinuous, the origin of the tensile residual strain is currently unknown.

Also shown in Figure 7 is the strain state of the Al_2Pt phase in the bond coat. Here the in-plane strains are less compressive than in the top coat which is consistent with the expected strain state due to thermal expansion mismatch.

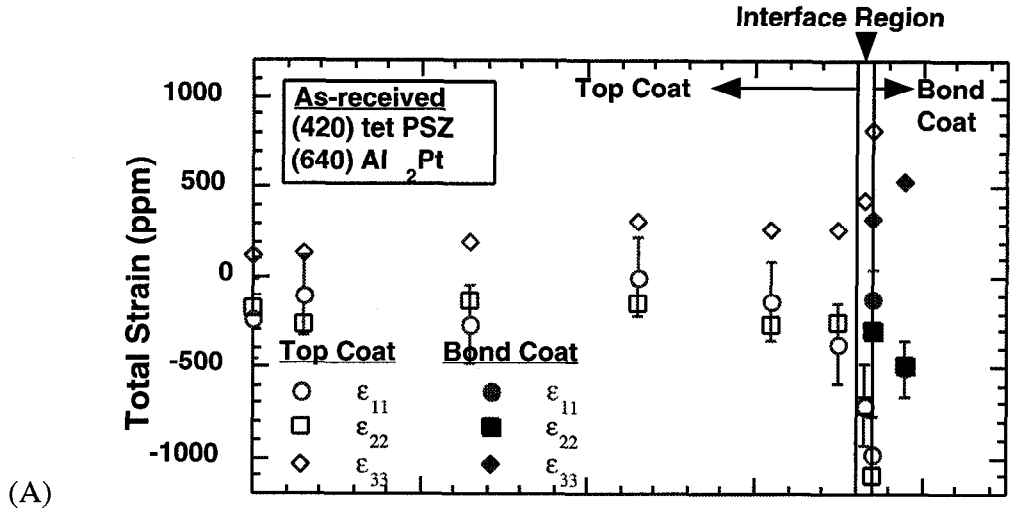

(A)

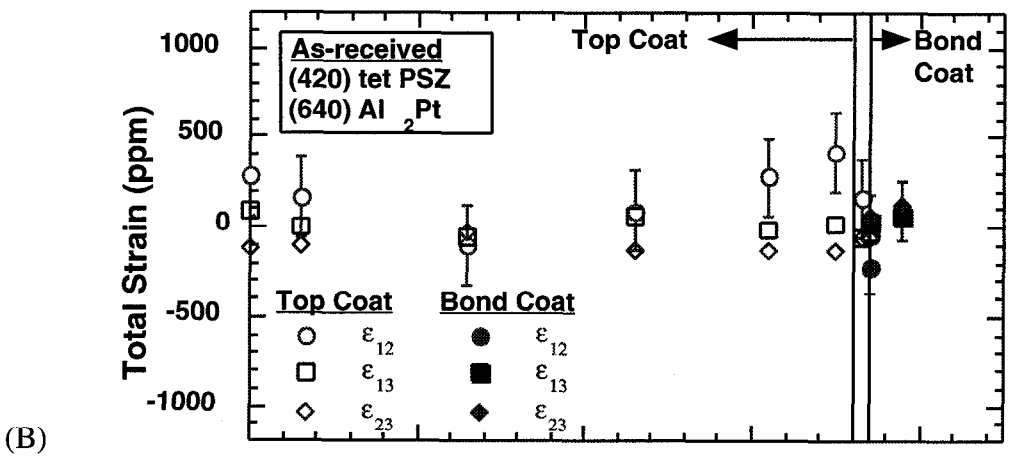

(B)

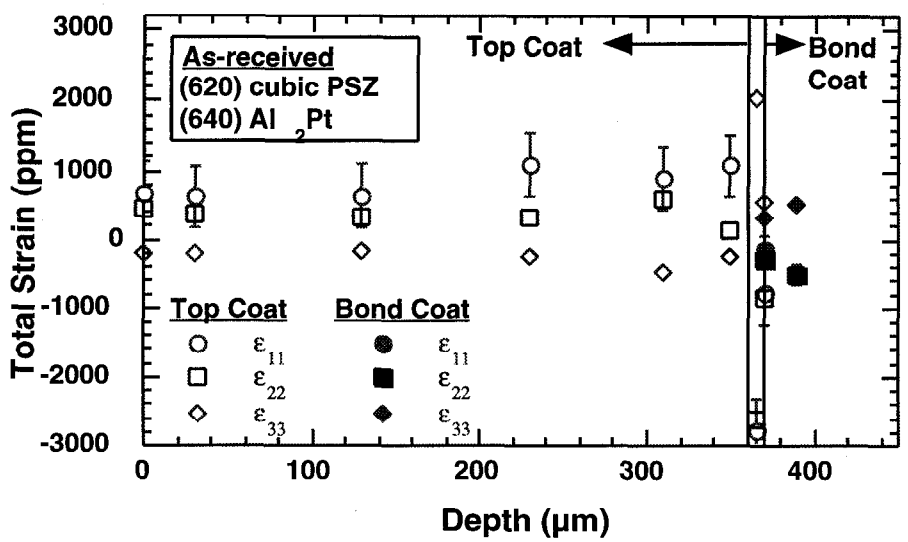

(C)

Figure 7. Total residual strain as a function of depth in the as-received specimen. Normal components of strain (ε_{ii}) in tetragonal YSZ and Al_2Pt (A), shear components of strain (ε_{ij}) in tetragonal YSZ and Al_2Pt (B), and normal components of strain (ε_{ii}) in cubic YSZ (C).

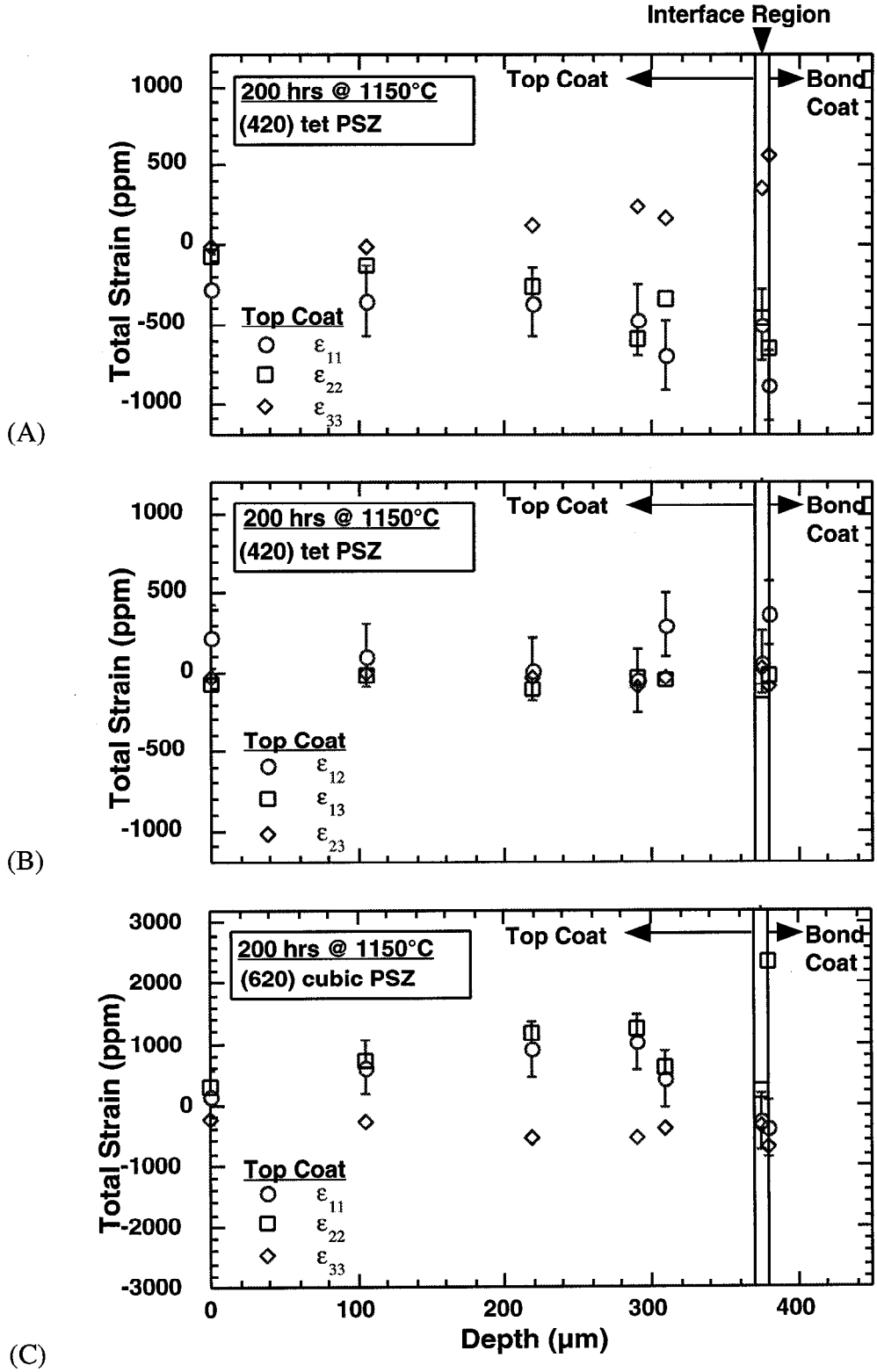

Figure 8. Total residual strain as a function of depth in the heat treated specimen. Normal components of strain (ε_{ii}) in tetragonal YSZ (A), shear components of strain (ε_{ij}) in tetragonal YSZ (B), and normal components of strain (ε_{ii}) in cubic YSZ (C).

SUMMARY

The residual strain states of the tetragonal and cubic phases were measured for EB-PVD YSZ top coat/(Pt,Ni)Al bond coat/René N5 single crystal substrate specimens before and after 200 hrs at 1150 °C. The magnitudes of the in-plane compressive strains in the tetragonal YSZ phase were small far away from the top coat/bond coat interface but increased as expected near the interface for both the as-received and heat treated specimens. This was not the case for the strain state of the cubic YSZ phase after heat treatment. The cubic YSZ exhibited significant in-plane tension near the interface.

ACKNOWLEDGMENTS

The authors wish to thank Dr. B. A. Nagaraj of G.E. Aircraft Engines for providing the specimens used in this study. Research sponsored by the U. S. Department of Energy, Assistant Secretary for Energy Efficiency and Renewable Energy, Office of Industrial Technologies, Industrial Energy Efficiency Division and Advanced Turbine Systems Program. Research facilities sponsored by the Assistant Secretary for Energy Efficiency and Renewable Energy, Office of Transportation Technologies, as part of the High Temperature Materials Laboratory User Program. Oak Ridge National Laboratory is managed by Lockheed Martin Energy Research Corp. for the U.S. Department of Energy under contract number DE-AC05-96OR22464.

REFERENCES

1. J. T. DeMasi-Marcin and D. K. Gupta, "Protective Coatings for the Gas Turbine Engine," Surf. Coat. Tech. **68/69** 1-9 (1994).
2. P. Bengtsson and T. Johannesson, "Modelled and Measured Residual Stresses in Plasma Sprayed Thermal Barrier Coatings," J. Thermal Spray Techn. **4** [3] 245-51 (1995).
3. P. Bengtsson and C. Persson, "Characterization and Microstructural Defects in Plasma Sprayed Thermal Barrier Coatings," to be published.
4. D. W. Jordan and K. T. Faber, " X-ray Residual Stress Analysis of a Ceramic Thermal Barrier Coating Undergoing Thermal Cycling," Thin Solid Films **235** 137-41 (1993).
5. H. Krause and A. Haase, "X-Ray Diffraction System PTS for Powder, Texture and Stress Analysis," pp. 405-8 in Experimental Techniques of Texture Analysis. Edited by H. J. Bunge, DGM Informationsgesellschaft•Verlag, 1986.
6. I. C. Noyan and J. B. Cohen, Residual Stress, Measurement by Diffraction and Interpretation, Springer-Verlag, New York, 1987, A, p. 101; B, pp. 126-30 and C, pp. 125-6.
7. A. Abuhasan, C. Balasingh and P. Predecki, "Residual Stresses in Alumina/Silicon Carbide (Whisker) Composites by X-ray Diffraction," J. Am. Ceram. Soc. **73** [8] 2474-84 (1990).
8. L. C. Hammond and J. L. Cocking, "Rietveld Analysis of Plasma-Sprayed PSZ Coatings," Powder Diffr. **11** [2] 75-9 (1996).
9. R. A. Miller, J. L. Smialek, and R. Garlick, "Phase Stability in Plasma-Sprayed, Partially Stabilized Zirconia-Yttria," pp. 241-53 in Science and Technology of Zirconia, Advances in Ceramics, V. 3. Edited by A. H. Heuer and L. W. Hobbs, The American Ceramic Society, Westerville, OH, 1981.
10. Powder Diffraction File, Sets 1-45, International Centre for Diffraction Data, Newton Square, PA 19073-3272, U.S.A.
11. Residual Stress Measurement by X-Ray Diffraction-SAE J784a, SAE, Warrendale, PA, 1980, pp. 63-4.